Light: Science & Applications (2013) 2, e76; doi:10.1038/lsa.2013.32

www.nature.com/lsa

REVIEW

Strong light–matter interaction in ZnO microcavities

Ying-Yu Lai, Yu-Pin Lan and Tien-Chang Lu

The strong light–matter interaction in ZnO-embedded microcavities has received great attention in recent years, due to its ability to generate the robust bosonic quasiparticles, exciton-polaritons, at or above room temperature. This review introduces the strong coupling effect in ZnO-based microcavities and describes the recent progress in this field. In addition, the report contains a systematic analysis of the room-temperature strong-coupling effects from relaxation to polariton lasing. The stable room temperature operation of polaritonic effects in a ZnO microcavity promises a wide range of practical applications in the future, such as ultra-low power consumption coherent light emitters in the ultraviolet region, polaritonic transport, and other fundamental of quantum optics in solid-state systems.
Light: Science & Applications (2013) **2,** e76; doi:10.1038/lsa.2013.32; published online 21 June 2013

Keywords: microcavity; polariton; strong coupling; ZnO

INTRODUCTION

Over the past two decades, strong light–matter interactions in solid-state systems have garnered much attention for applications in novel photonics devices. The polariton is the key factor in the strong coupling phenomena: a new bosonic quasiparticle that is a hybrid between matter and light and exhibits promise for investigating various fascinating effects including dynamical Bose condensation,[1–4] superfluidity[5,6] and quantized vortices.[7–10] Semiconductor microcavities (MCs), which simultaneously offer good optical confinement with a small mode volume for the photonics portion and an excitonic layer for the matter portion of the strong coupling, are regarded as promising candidates for demonstrating and manipulating strong light–matter coupling in solid-state systems.[11] Because the semiconductor MCs undergo a strong coupling regime, the coupling rate between the bared exciton modes and the confined photon modes is faster than their dissipation rates. Compared with weakly coupled MCs, the rapid exchange rate in strongly coupled MCs renders the energy transfer between the excitons and photons reversible and reduces the possibility of energy dissipation through non-radiative channels, which results in a higher internal quantum efficiency. The new eigenstates generated from the strong exciton–photon coupling are called exciton-polaritons[12] and exhibit a relatively small effective mass compared with atomic hydrogen, tunable dispersion curves, and the bosonic statistics at low densities.

Given the aforementioned properties, many phenomena have been extensively studied in polariton systems, including ultra-low threshold polariton lasing,[13] polariton parametric oscillation[14–17] and polaritonic circuits.[18] The matter characteristic of the polaritons allows them to scatter with electrons, phonons and polaritons, then to condense in the coherent ground state. The laser-like light emission from a coherent polariton ground state, the so-called polariton laser, does not require the population inversion condition required by conventional semiconductor lasers. The critical temperatures of the polariton condensate could even be elevated to room temperature, a basic condition for practical applications, due to the extremely small effective mass of the polaritons.

PROGRESS HISTORY

Due to the rapid development of semiconductor fabrication capabilities, the bared excitons can couple with the various types of photon modes that are confined in different semiconductor MCs, including the whispering-gallery mode in microtapers,[19] microwires[20] and microrods,[21] the waveguide mode in semiconductor nanowires,[22,23] the photonic crystal modes,[24–26] and the most-often used Fabry-Perot mode in planar MCs.[27] From a more realistic perspective, a planar MC is more easily fabricated and applied to electrical devices, making it a more attractive choice for future practical applications such as ultra-low threshold polariton lasing. Therefore, the following paragraph focuses on the planar MC structure and the polariton lasing achieved by the systems of different materials.

The first demonstration of exciton-polaritons in a planar semiconductor MC was produced using the GaAs system by Weisbuch *et al.*[27] Since then, several reports on polariton lasing, the most appealing polaritonic application, have involved planar semiconductor MCs. During the early twenty-first century, polariton lasers were demonstrated at cryogenic temperatures in GaAs[28] and CdTe[13] MCs due to their small exciton binding energies. Thus, a portion of the polariton laser research attention was transferred to wide-bandgap material systems, including GaN and ZnO, which provide a much higher exciton binding energy and oscillator strength for supporting stable room-temperature (RT) operation. Thus far, the GaN-based polariton lasers have been demonstrated in planar MCs inserted with different types of excitonic structures including bulk GaN,[29] GaN/AlGaN multiple quantum wells (MQWs)[30] and GaN nanowires.[31] The exciton binding

Department of Photonics, National Chiao Tung University, Hsinchu 300
Correspondence: TC Lu, Department of Photonics, National Chiao Tung University, Hsinchu 300
E-mail: timtclu@mail.nctu.edu.tw
Received 18 September 2012; revised 18 January 2013; accepted 18 January 2013

energy of the bulk GaN is comparable to the RT thermal energy of approximately 26 meV. Although the exciton binding energy can reach approximately 40 meV in the GaN/AlGaN MQW system, the oscillator strength is reduced due to the poor wave function overlap caused by the quantum-confined Stark effect on the commonly used c-plane substrates.[32] A large number of QWs is required to increase the oscillator strength and maintain the strong coupling regime, but this requirement causes difficulties with the epitaxy. On the other hand, the nanowire separation density in the MC is more difficult to control during the fabrication of the GaN nanowire-embedded MCs, making future practical applications more difficult.

To examine a more reliable polariton operation, ZnO provides an appealing material, because it possesses exciton binding energies that are twice as large as (approximately 60 meV in the bulk layer) and coupling strengths that are comparable to those in the GaN system. Thus, ZnO is the most adaptive candidate for stable polariton operation at RT. Since the pioneering work on the strong coupling effect in ZnO planar MCs reported by Shimada *et al.*,[33] several other groups have reported on the characteristics of strongly coupled ZnO MCs.[34–37] In 2011, the first polariton lasing in the bulk ZnO planar MC was demonstrated by Guillet *et al.*[38] at 120 K with a small negative detuning. Later, Franke *et al.*[39] pushed the operation temperature of the ZnO polariton lasing up to 250 K by depositing a polycrystalline ZnO inside two dielectric distributed Bragg reflectors (DBRs). One month later, Lu *et al.*[40] successfully demonstrated the first RT polariton lasing in ZnO-based hybrid microcavities with an ultra-low threshold. Das *et al.*[41] followed with a method similar to that in their previous report on GaN nanowire MCs and observed polariton lasing in a fully dielectric DBR-based MC. Recently, Lai *et al.*[42] observed polariton lasing in hybrid ZnO microcavities at the even higher temperature of 353 K and verified its coherence properties.

POLARITONIC EFFECTS IN A ZINC OXIDE MICROCAVITY

A series of strong light–matter interaction phenomena in a ZnO-based MC are described in this study. Details from the fabrication to the measurements are provided. The relaxation process and bottleneck effect of the polariton at different exciton–photon detunings are verified using temperature- and power-dependent photoluminescence (PL). Moreover, the report described both the polariton lasing in the strong coupling regime achieved by the polariton–polariton scattering with increasing pumping power and the photon lasing in the weak coupling regime resulting from the collapse of the strong coupling regime that was observed in the different positions of the sample at RT.

FABRICATIONS AND METHODS

Figure 1a provides a schematic diagram of the hybrid MC structure consisting of a bulk ZnO $3\lambda/2$-thick cavity sandwiched between a bottom AlN/$Al_{0.23}Ga_{0.77}N$ DBR and a top dielectric SiO_2/HfO_2 DBR. The 30-pair AlN/AlGaN DBR and a GaN buffer layer were grown using an EMCORE D75 metal-organic chemical vapor deposition system on a (0001)-oriented sapphire substrate. Trimethylgallium (TMGa) and trimethylaluminum (TMAl) were used as the group III source materials and ammonia (NH_3) as the group V source material. The growth pressure was maintained at 100 torr. To achieve a high reflectivity epitaxial DBR with a wide stop-band width, we inserted six-period GaN/AlN super lattice layers into every 3 to 5 AlN/AlGaN DBR pairs to suppress the tensile strain in the epitaxial DBR.[43] The $3\lambda/2$-thick ZnO cavity layer was then grown on the AlN/$Al_{0.23}Ga_{0.77}N$ epitaxial DBR using a pulsed KrF excimer laser (λ=248 nm) deposition system. Atomic force microscopy (AFM) was employed to investigate the structural quality of the ZnO layer. Figure 1b provides the AFM image with a low root mean square (rms) roughness of R_{rms}=1.7 nm. The thickness gradient of the epitaxial ZnO layer and the AlN/AlGaN DBR provide various detunings at the same sample to prevent process inaccuracies between the different samples. Finally, the 9-period SiO_2/HfO_2 dielectric DBR was coated onto the ZnO layer *via* electron-gun deposition to complete the MC structure. The corresponding cross-sectional scanning electron microscopy image of the complete MC is shown in Figure 1c.

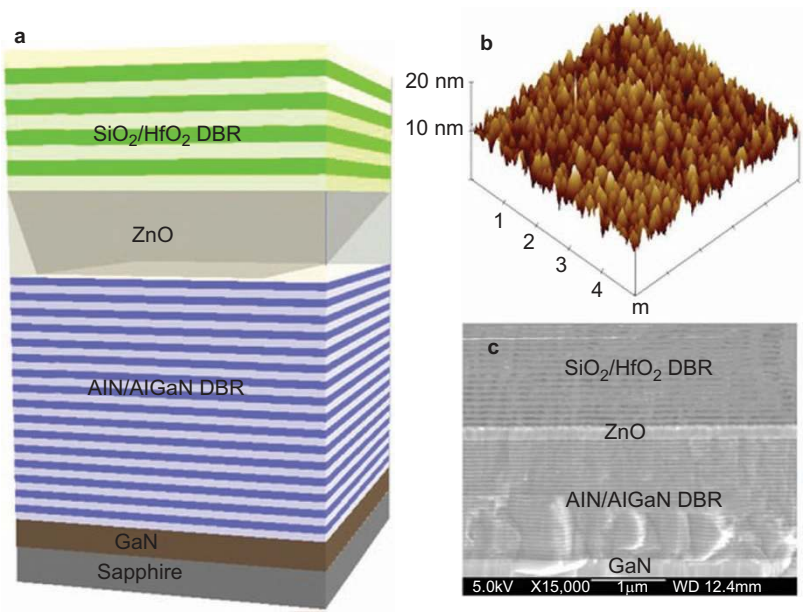

Figure 1 (**a**) Schematic diagram of the hybrid ZnO MC. (**b**) AFM image of the ZnO cavity. (**c**) Cross-sectional scanning electron microscopy image of the ZnO MC. AFM, atomic force microscopy; MC, microcavity.

doi:10.1038/lsa.2013.32

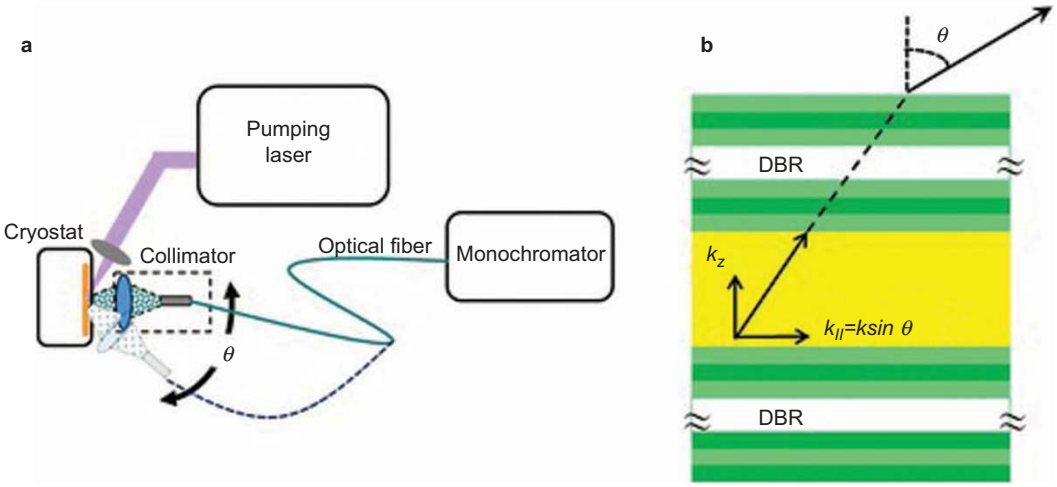

Figure 2 Schematic diagrams of (**a**) the ARPL measurement and (**b**) the one-to-one correspondence between the internal polaritons and the external photons. ARPL, angle-resolved photoluminescence.

The dispersion relationships of the exciton-polaritons in the ZnO MC were first investigated using angle-resolved photoluminescence (ARPL) measurements as shown in Figure 2a. This technique relies on a one-to-one correspondence between each internal lower polariton (LP) at $k_{//}$ and each external photon emitted at θ with the same $k_{//}$ and $E_{LP}(k_{//})$ (Figure 2b). Thus, the in-plane polariton information could be collected by increasing the observation angle of the optical fiber and the detuning parameter between the cavity photons and the excitons. The polariton relaxation mechanisms could be specified from the ARPL measurement using several methods such as adjusting the exciton–photon detuning to a different position on the sample, changing the operation temperature, or increasing the pumping power.

RELAXATION PROCESS AND THE BOTTLENECK EFFECT

Given the hybrid nature of the light and matter in the exciton-polaritons, their matter portion allowed the hot polaritons at a high k state

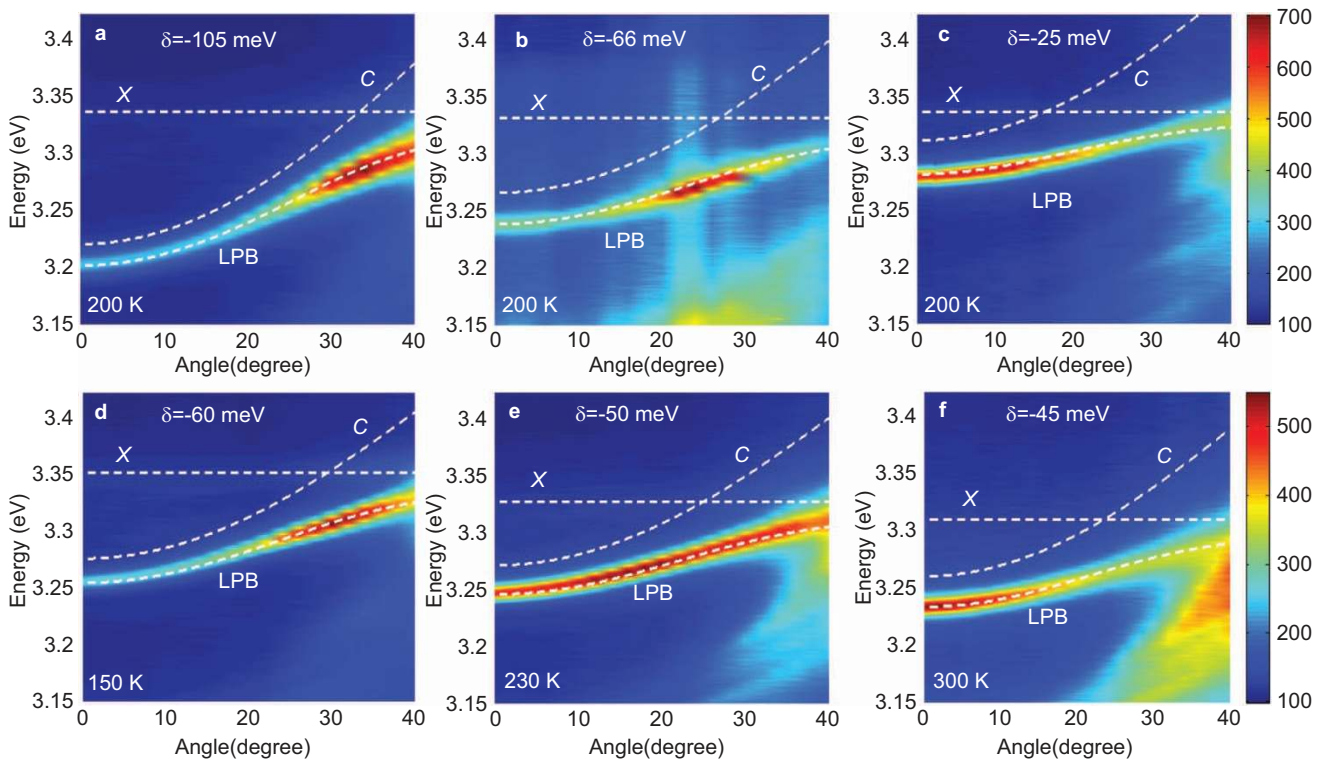

Figure 3 Color maps of the ARPL measurements for the different positions on the ZnO hybrid MC sample with three different detunings: (**a**) $\delta=-105$ meV, (**b**) $\delta=-66$ meV and (**c**) $\delta=-25$ meV at 200 K. (**d**)–(**f**) The dispersion relationships at the same position with increasing temperature from 150 to 300 K. The uncoupled cavity mode (*C*), exciton mode (*X*) and LPB (white dashed line) fitted from the coupled oscillator model are plotted for reference. ARPL, angle-resolved photoluminescence; LPB, lower polariton branch; MC, microcavity.

to relax to a low k state through polariton–polariton scattering and polariton–phonon scattering. Thus, the relaxation of the polaritons strongly depended on the exciton-photon detuning ($\delta = Ex - Ec$) which determines the exciton and photon composition of the polariton states. Herein, three types of detuning were measured at different positions on the ZnO hybrid MC sample below 200 K with a low pumping power density of 50 W cm^{-2} using the 266-nm emission from the fourth harmonics of a Nd:YAG pulsed laser with a 5-ns pulse duration and a 50-kHz repetition rate to avoid the polariton–polariton scattering effect. The lower polariton branch (LPB) in the dispersion relationship exhibited a near-parabolic distribution at small angles and converged onto the bared exciton energy at large angles, which depicts the anti-crossing behavior and the hybrid nature of the strong light–matter interaction between the exciton and the cavity photon characteristics.

The dispersion curves in Figures 3–5 were analyzed using the coupled oscillator model, and the labels *X*, *C* and LPB represent the exciton mode, the cavity mode and the lower polariton branch, respectively. Figure 3a shows the larger negative detuning case ($\delta = -105$ meV) with a 112 meV Rabi splitting. The polaritons accumulated at 35° reveal a commonly seen relaxation bottleneck effect, which can be attributed to the low exciton fraction of the LPB and reflects the reduced possibility for the hot polaritons to cool down *via* scattering with the phonons. Therefore, the bottleneck effect could be suppressed by more efficient polariton–phonon scattering in a smaller negative detuning case in which the LPB is more exciton-like.

Figure 3b presents the dispersion relationship of polaritons at different positions with a smaller detuning $\delta = -66$ meV in which the maximum intensity of the LPB occurred at 25°, suggesting a more efficient polariton relaxation than that depicted in Figure 3a. Moreover, the polaritons were thermalized to the low k state of the LPB in an even smaller negative detuning case ($\delta = -25$ meV) as shown in Figure 3c. The exciton–photon detuning could also be adjusted by varying the operation temperature at the same position on the sample through a difference between the temperature-dependent refractive index and the exciton energy variation as shown in Figure 3d–3f. By increasing the temperature from 150 to 300 K, the detuning varied from −60 to −45 meV. The corresponding bottleneck effect was sufficiently suppressed by the stronger phonon-assisted relaxation due to the smaller detuning case with the higher exciton character and temperature that provided a more sufficient phonon scattering rate.

POLARITON LASING AT ROOM TEMPERATURE

The polaritons can be observed using the temperature-dependent measurements and are stable even at RT in the ZnO MC due to their large exciton-binding energy and oscillator strength. At RT, the thermally activated escape mechanism of the ground state polaritons is stronger and can compete with the polariton relaxation process.[44] Therefore, a deeper polariton trap formed by a larger negative detuning is essential for preventing the ground-state polaritons from escaping through thermal energy. Thus, we performed an ARPL measurement with a frequency-tripled Nd:YVO_4 pulsed laser at two different detunings, $\delta = -109$ meV and $\delta = -39$ meV, to better demonstrate the RT polariton lasing.

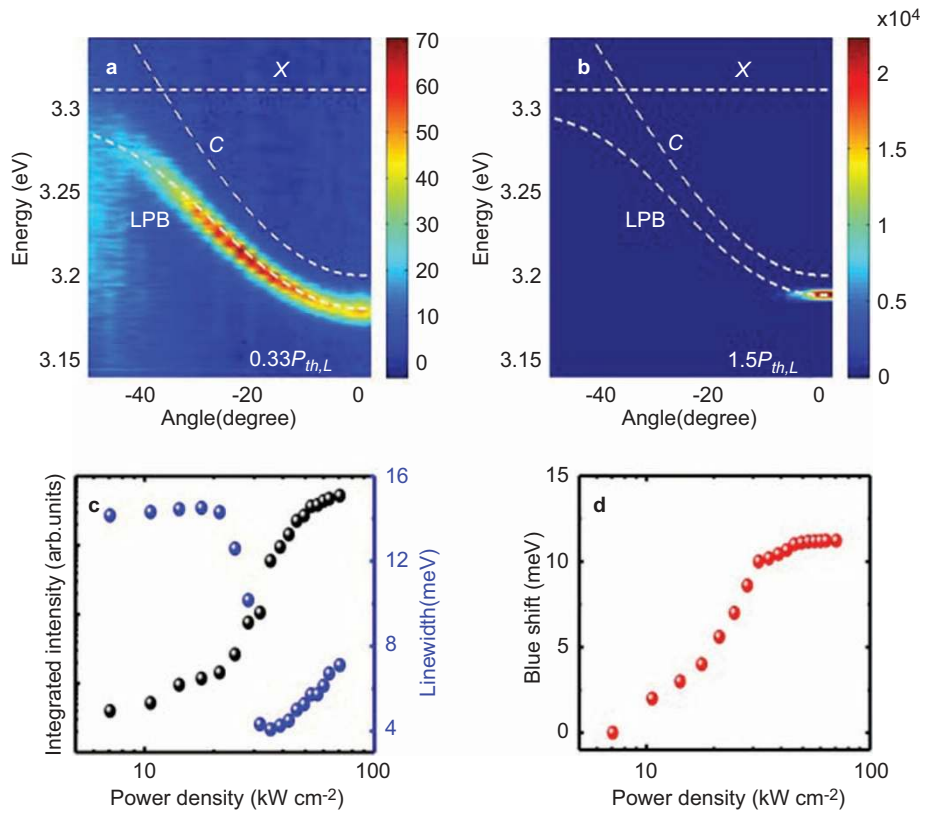

Figure 4 The color maps of the angular dispersions from the measured PL spectra at (**a**) 0.33$P_{th,L}$ and (**b**) 1.5$P_{th,L}$ for the case of $\delta = -109$ meV at RT. (**c**) The integrated emission intensity and emission linewidth and (**d**) the energy blueshift of the polariton versus the pumping density for the large detuning case ($\delta = -109$ meV) at RT. PL, photoluminescence; RT, room temperature.

doi:10.1038/lsa.2013.32

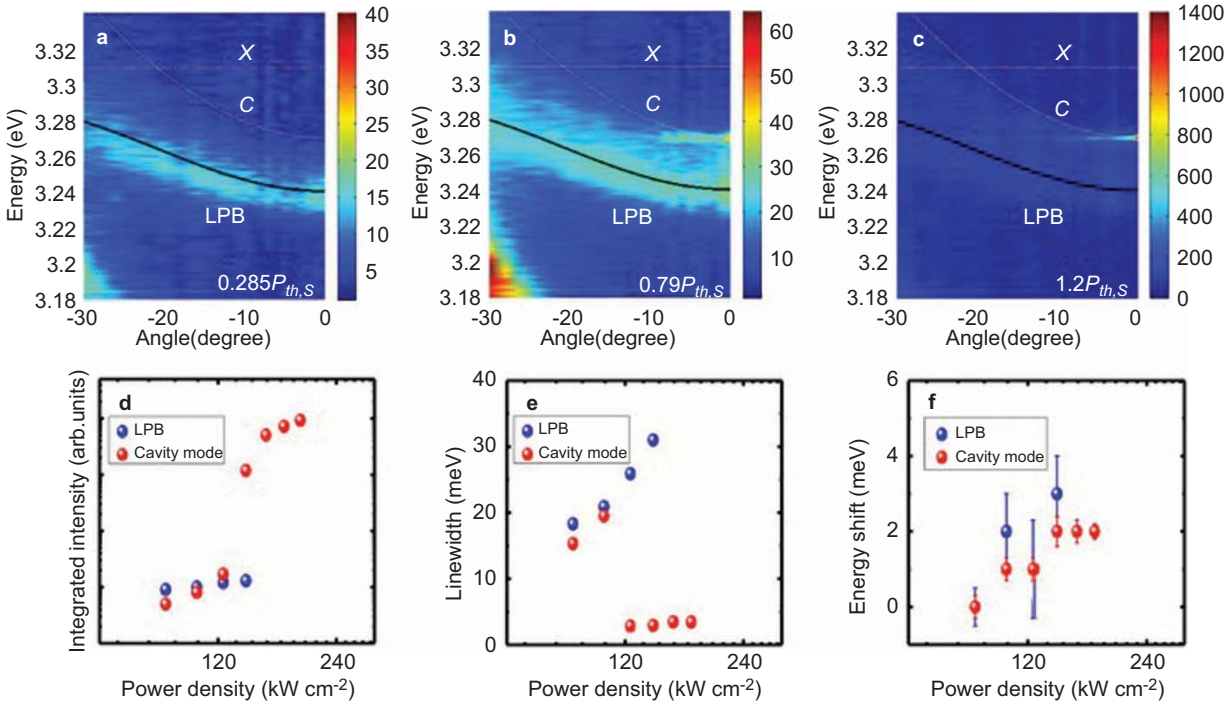

Figure 5 The color maps of the angular dispersions from the measured PL spectra at (**a**) 0.285$P_{th,S}$, (**b**) 0.79$P_{th,S}$ and (**c**) 1.2$P_{th,S}$ for the case of $\delta=-39$ meV at RT. The coexistence of the LPB and the cavity mode can be observed in (**b**) due to the collapse of the strong coupling regime at the central region of the Gaussian-shaped pumping spot. (**d**) The integrated emission intensity, (**e**) emission linewidth and (**f**) energy blueshift of the LPB (larger blue spheres) and cavity mode (smaller red spheres) versus the pumping density for the small detuning case ($\delta=-39$ meV) at RT. LPB, lower polariton branch; PL, photoluminescence; RT, room temperature.

Figure 4a shows a large negatively detuned case ($\delta=-109$ meV) with a Rabi splitting of approximately 102 meV at a low pumping energy density. Although phonon-assisted relaxation was involved, the relaxation bottleneck persisted at a large negative detuning. By increasing the pumping power, the bottleneck was suppressed *via* the polariton–polariton scattering as shown in Figure 4b. In addition, the nonlinear increase in the ground-state polariton emission intensity was attributed to the polariton lasing as shown in Figure 4b. The power-dependent measurements indicated that the threshold was approximately $P_{th,L}=21.2$ kW cm^{-2}, which corresponds to a carrier density of 1.66×10^{17} cm^{-3} and is below the Mott density in ZnO.[45] The significant reduction in the polariton linewidth from 14 to 4 meV at the nonlinear threshold demonstrated the spontaneous coherence build-up of the polariton laser. The obvious linewidth broadening after the threshold demonstrated the decoherence mechanism induced by the polariton–polariton interaction. The expected polariton self-interaction-induced blueshift is also shown in Figure 4d.

THE TRANSITION FROM STRONG COUPLING REGIME TO WEAK COUPLING REGIME

Although phonon-assisted relaxation is more efficient in a smaller negative detuning regime ($\delta=-39$ meV), the polariton laser cannot be observed at pumping intensities above the threshold density of the larger negative detuning case primarily because the leakage rate of the ground-state polaritons through the thermally induced detrapping phenomena is faster than the injection rate of the polariton–polariton scattering and the polariton–phonon scattering. The corresponding dispersion relationship is shown in Figure 5a. With further increases in the pumping power, a second peak emerged at the cavity mode, which corresponded to the transition from the strong coupling regime to the weak coupling regime as shown in Figure 5b. The residual LPB emission came from the edge emission of the Gaussian-shaped pumping spot, which had a smaller power density and persisted in the strong coupling regime. The conventional photon lasing, i.e., the vertical cavity surface-emitting laser operation, can be observed in Figure 5c with a nonlinear increase in the emission intensity. The threshold power density derived from Figure 5d was $P_{th,S}=123.67$ kW cm^{-2}. The corresponding carrier density was approximately 9.7×10^{17} cm^{-3}, which is higher than the Mott density in ZnO. Figure 5e indicates that the linewidth of the photon laser has no significant broadening compared with the polariton laser case. In addition, the lasing wavelength was fixed to the bare photon mode as shown in Figure 5f. The varying tendencies of the linewidth and blueshift reveal the completely different lasing mechanisms of the strong and weak coupling regimes in the ZnO MC.

DISTINGUISHING THE POLARIZATION

To further verify the different lasing mechanisms' effect on the polariton and the photon inside the microcavity, the polarization was measured from the direction normal to the ZnO MC sample using a rotational polarizer. Figure 6 shows the polarization characteristics of the polariton and photon lasers. In the c-plane ZnO bulk active layer, the exciton–exciton scattering should be spin-isotropic. Hence, the time-integrated spontaneous polarization of the polariton lasing exhibited a low degree of polarization (DOP).[46] For the photon lasing achieved in a small detuning region, the observed DOP approached 90%. The higher DOP with the photon lasing indicates that the polarization was dominated by the slight photonic disorder in the ZnO MC. No relationship was noted in the polarizations of the pumping laser and the output polariton/photon laser from the ZnO MC because the excitation differed greatly from the resonant energy.

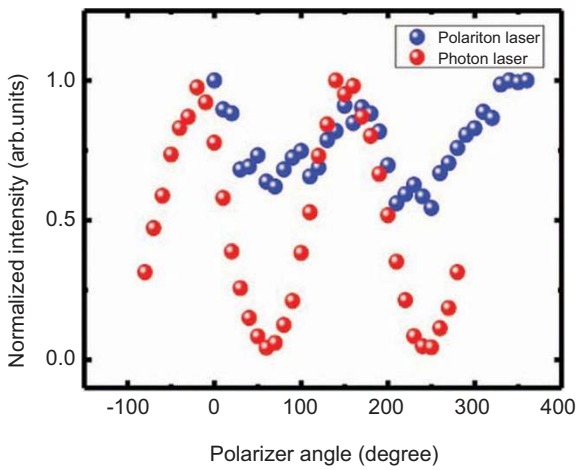

Figure 6 The polarization of the polariton and photon lasers above the threshold conditions.

CONCLUSION AND PROSPECTS

Many investigations of ZnO-based MCs have been undertaken since the strong coupling effects in the ZnO MCs were first reported in 2008.[33] We have reviewed the progress of investigations on the strongly coupled ZnO MCs and have briefly introduced the strong coupling effects from relaxation to polariton lasing in ZnO MCs. The RT polariton lasing was achieved with an extremely low threshold density at for the large negative detuning case, which had a deeper polariton trap to compete with the thermally activated escape process. Although several groups have demonstrated the strong light–matter interactions and the corresponding polariton lasers at RT in both hybrid and fully dielectric ZnO MCs, their performance remains limited by the imperfections in the ZnO layer's epitaxial quality and by the nitride-based DBR. However, these problems could be solved by using a high-quality single-crystal ZnO layer on the ZnO substrate accompanied by highly reflective dielectric DBRs.[47] To achieve this MC structure, the thickness of ZnO substrate must be reduced from several hundred micrometers to hundred nanometers using a dry-etching process and chemical–mechanical polishing. The photonic surface roughness of the etched side should be carefully polished, but the cavity thickness is difficult to control.

Another bothersome issue of the ZnO MC is that the upper polariton branch, a characteristic important in determining the strong coupling, is typically difficult to observe in the bulk ZnO system due to the strong absorption of the excitons in the thick ZnO layer.[48,49] Therefore, the excitonic layers could be altered to the ZnO/ZnMgO multiple quantum well to reduce the absorption length of the excitonic layer and to enhance the oscillator strength provided by the quantum-confined effect. In 2011, the strong coupling effect was reported by Halm *et al.*[50] and verified using the observable upper polariton branch in an all-epitaxial ZnO MQW MC at 5 K. Although the strong coupling effect collapsed at 150 K, which could be attributed to the thermal broadening of the excitons, the situation was improved by inserting more QW pairs or by improving the epitaxial quality of the MQWs. Thus, the MQW structure could combine with the ZnO substrate to yield a robust ultra-low-threshold coherent light source in the ultraviolet region. The strongly coupled ZnO MC provides great potential for future scientific research into RT quantum degenerate systems and the development of other practical polaritonic devices.

ACKNOWLEDGMENTS

The authors are grateful to Professor SC Wang, Professor WF Hsieh and Professor HC Kuo at the National Chiao Tung University for their kind support and to Professor H Deng at the University of Michigan for her helpful discussions. This work has been supported by the NSC in Taiwan under contract NSC 100-2628-E-009-013-MY3.

1 Deng H, Weihs G, Santori C, Bloch J, Yamamoto Y. Condensation of semiconductor microcavity exciton polaritons. *Science* 2002; **298**: 199–202.
2 Richard M, Kasprzak J, Romestain R, André R, Dang LS. Spontaneous coherent phase transition of polaritons in CdTe microcavities. *Phys Rev Lett* 2005; **94**: 187401.
3 Kasprzak J, Richard M, Kundermann S, Baas A, Jeambrun P *et al*. Bose–Einstein condensation of exciton polaritons. *Nature* 2006; **443**: 409–414.
4 Balili R, Hartwell V, Snoke D, Pfeiffer L, West K. Bose–Einstein condensation of microcavity polaritons in a trap. *Science* 2007; **316**: 1007–1010.
5 Amo A, Lefrère J, Pigeon S, Adrados C, Ciuti C *et al*. Superfluidity of polaritons in semiconductor microcavities. *Nat Phys* 2009; **5**: 805–810.
6 Sanvitto D, Marchetti FM, Szymańska MH, Tosi G, Baudisch M *et al*. Persistent currents and quantized vortices in a polariton superfluid. *Nat Phys* 2010; **6**: 527–533.
7 Lagoudakis KG, Wouters M, Richard M, Baas A, Carusotto I *et al*. Quantized vortices in an exciton-polariton condensate. *Nat Phys* 2008; **4**: 706–710.
8 Lagoudakis KG, Ostatnický T, Kavokin AV, Rubo YG, André R *et al*. Observation of Half-Quantum Vortices in an Exciton-Polariton Condensate. *Science* 2009; **326**: 974–976.
9 Roumpos G, Fraser MD, Löffler A, Höfling S, Forchel A *et al*. Single vortex-antivortex pair in an exciton-polariton condensate. *Nat Phys* 2011; **7**: 129–133.
10 Nardin G, Grosso G, Léger Y, Piętka B, Morier-Genoud F *et al*. Hydrodynamic nucleation of quantized vortex pairs in a polariton quantum fluid. *Nat Phys* 2011; **7**: 635–641.
11 Vahala KJ. Optical microcavities. *Nature* 2003; **424**: 839–846.
12 Hopfield. Theory of the contribution of excitons to the complex dielectric constant of crystals. *Phys Rev* 1958; **112**: 1555–1567.
13 Huang R, Yamamoto Y, André R, Bleuse J, Muller M *et al*. Exciton-polariton lasing and amplification based on exciton–exciton scattering in CdTe microcavity quantum wells. *Phys Rev B* 2002; **65**: 165314.
14 Baumberg JJ, Savvidis PG, Stevenson RM, Tartakovskii AI, Skolnick MS *et al*. Parametric oscillation in a vertical microcavity: a polariton condensate or micro-optical parametric oscillation. *Phys Rev B* 2000; **62**: 16247–16250.
15 Saba M, Ciuti C, Bloch J, Thierry-Mieg V, André R *et al*. High-temperature ultrafast polariton parametric amplification in semiconductor microcavities. *Nature* 2001; **414**: 731–735.
16 Diederichs C, Tignon J, Dasbach G, Ciuti C, Lemaître A *et al*. Parametric oscillation in vertical triple microcavities. *Nature* 2006; **440**: 904–907.
17 Ferrier L, Pigeon S, Wertz E, Bamba M, Senellart P *et al*. Polariton parametric oscillation in a single micropillar cavity. *Appl Phys Lett* 2010; **97**: 031105.
18 Liew TCH, Kavokin AV, Shelykh IA. Optical circuits based on polariton neurons in semiconductor microcavities. *Phys Rev Lett* 2008; **101**: 016402.
19 Sun LX, Chen ZH, Ren QJ, Yu K, Bai LH *et al*. Direct observation of whispering gallery mode polaritons and their dispersion in a ZnO tapered microcavity. *Phys Rev Lett* 2008; **100**: 156403.
20 Trichet A, Sun L, Pavlovic G, Gippius NA, Malpuech G *et al*. One-dimensional ZnO exciton polaritons with negligible thermal broadening at room temperature. *Phys Rev B* 2011; **83**: 041302.
21 Dai J, Xu CX, Sun XW, Zhang XH. Exciton-polariton microphotoluminescence and lasing from ZnO whispering-gallery mode microcavities. *Appl Phys Lett* 2011; **98**: 161110.
22 Vugt LKv, Piccione B, Cho CH, Nukala P, Agarwal R. One-dimensional polaritons with size-tunable and enhanced coupling strengths in semiconductor nanowires. *Proc Nat Acad Sci* 2011; **108**: 10050–10055.
23 Vugt LKv, Rühle S, Ravindran P, Gerritsen HC, Kuipers L *et al*. Exciton polaritons confined in a ZnO nanowire cavity. *Phys Rev Lett* 2006; **97**: 147401.
24 Nomura M, Kumagai N, Iwamoto S, Ota Y, Arakawa Y. Laser oscillation in a strongly coupled single-quantum-dot-nanocavity system. *Nat Phys* 2010; **6**: 279–283.
25 Ohta R, Ota Y, Nomura M, Kumagai N, Ishida S *et al*. Strong coupling between a photonic crystal nanobeam cavity and a single quantum dot. *Appl Phys Lett* 2011; **98**: 173104.
26 Azzini S, Gerace D, Galli M, Sagnes I, Braive R *et al*. Ultra-low threshold polariton lasing in photonic crystal cavities. *Appl Phys Lett* 2011; **99**: 111106.
27 Weisbuch C, Nishioka M, Ishikawa A, Arakawa Y. Observation of the coupled exciton-photon mode splitting in a semiconductor quantum microcavity. *Phys Rev Lett* 1992; **69**: 3314–3317.
28 Deng H, Weihs G, Snoke D, Bloch J, Yamamoto Y. Polariton lasing *vs.* photon lasing in a semiconductor microcavity. *Proc Nat Acad Sci* 2003; **100**: 15318–15323.
29 Christopoulos S, Baldassarri Höger von Högersthal G, Grundy AJD, Lagoudakis PG, Kavokin AV *et al*. Room-temperature polariton lasing in semiconductor microcavities. *Phys Rev Lett* 2007; **98**: 126405.

doi:10.1038/lsa.2013.32

30 Christmann G, Butté R, Feltin E, Carlin J, Grandjean N. Room temperature polariton lasing in a GaN/AlGaN multiple quantum well microcavity. *Appl Phys Lett* 2008; **93**: 051102.
31 Das A, Heo J, Jankowski M, Guo W, Zhang L *et al*. Room temperature ultralow threshold GaN nanowire polariton laser. *Phys Rev Lett* 2011; **107**: 066405.
32 Leroux M, Grandjean N, Laügt M, Massies J, Gil B *et al*. Quantum confined Stark effect due to built-in internal polarization fields in (Al,Ga)N/GaN quantum wells. *Phys Rev B* 1998; **58**: R13371–R13374.
33 Shimada R, Xie J, Avrutin V, Özgür Ü, Morkoč H. Cavity polaritons in ZnO-based hybrid microcavities. *Appl Phys Lett* 2008; **92**: 011127.
34 Chen JR, Lu TC, Wu YC, Lin SC, Liu WR *et al*. Large vacuum Rabi splitting in ZnO-based hybrid microcavities observed at room temperature. *Appl Phys Lett* 2009; **94**: 061103.
35 Sturm C, Hilmer H, Schmidt-Grund R, Grundmann M. Observation of strong exciton-photon coupling at temperatures up to 410K. *New J Phys* 2009; **11**: 073404.
36 Chen JR, Lu TC, Wu YC, Lin SC, Hsieh WF *et al*. Characteristics of exciton-polaritons in ZnO-based hybrid microcavities. *Opt Express* 2011; **19**: 4101–4112.
37 Orosz L, Réveret F, Bouchoule S, Zúñiga-Pérez J, Médard F *et al*. Fabrication and optical properties of a fully-hybrid epitaxial ZnO-based microcavity in the strong coupling regime. *Appl Phys Express* 2011; **4**: 072001.
38 Guillet T, Mexis M, Levrat J, Rossbach G, Brimont C *et al*. Polariton lasing in a hybrid bulk ZnO microcavity. *Appl Phys Lett* 2011; **99**: 161104.
39 Franke H, Sturm C, Schmidt-Grund R, Wagner G, Grundmann M. Ballistic propagation of exciton–polariton condensates in a ZnO-based microcavity. *New J Phys* 2012; **14**: 013037.
40 Lu TC, Lai YY, Lan YP, Huang SW, Chen JR *et al*. Room temperature polariton lasing vs. photon lasing in a ZnO-based hybrid microcavity. *Opt Express* 2012; **20**: 5530–5537.
41 Das A, Heo J, Bayraktaroglu A, Guo W, Ng TK *et al*. Room temperature strong coupling effects from single ZnO nanowire microcavity. *Opt Express* 2012; **20**: 11830–11837.
42 Lai YY, Lan YP, Lu TC. High temperature polariton lasing in a strongly coupled ZnO microcavity. *Appl Phys Express* 2012; **5**: 082801.
43 Huang GS, Lu TC, Yao HH, Kuo HC, Wang SC. Crack-free GaN/AlN distributed Bragg reflectors incorporated with GaN/AlN superlattices grown by metalorganic chemical vapor deposition. *Appl Phys Lett* 2006; **88**: 061904.
44 Levrat J, Butté R, Christmann G, Feltin E, Carlin J *et al*. Tailoring the strong coupling regime in III-nitride based microcavities for room temperature polariton laser applications. *Phys Status Solidi C* 2009; **6**: 2820–2827.
45 Klingshirn C, Fallert J, Zhou H, Sartor J, Thiele C *et al*. 65 years of ZnO research – old and very recent results. *Phys Status Solidi B* 2010; **247**: 1424–1447.
46 Baumberg JJ, Kavokin AV, Christopoulos S, Grundy AJD, Butté R *et al*. Spontaneous polarization buildup in a room-temperature polariton laser. *Phys Rev Lett* 2008; **101**: 136409.
47 Li F, Orosz L, Kamoun O, Bouchoule S, Brimont C *et al*. ZnO-based polariton laser operating at room temperature: from excitonic to photonic condensate. arXiv:1207.7172.
48 Faure S, Guillet T, Lefebvre P, Bretagnon T, Gil B. Comparison of strong coupling regimes in bulk GaAs, GaN, and ZnO semiconductor microcavities. *Phys Rev B* 2008; **78**: 23523.
49 Lin SC, Chen JR, Lu TC. Broadening of upper polariton branch in GaAs, GaN, and ZnO semiconductor microcavities. *Appl Phys B* 2011; **103**: 137–144.
50 Halm S, Kalusniak S, Sadofev S, Wünsche HJ, Henneberger F. Strong exciton–photon coupling in a monolithic ZnO/(Zn,Mg)O multiple quantum well microcavity. *Appl Phys Lett* 2011; **99**: 181121.